Acta Pharmaceutica Sinica B 2025;15(3):1643−1658

Chinese Pharmaceutical Association
Institute of Materia Medica, Chinese Academy of Medical Sciences

Acta Pharmaceutica Sinica B

www.elsevier.com/locate/apsb
www.sciencedirect.com

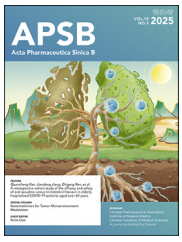

ORIGINAL ARTICLE

USP25 ameliorates vascular remodeling by deubiquitinating FOXO3 and promoting autophagic degradation of FOXO3

Yanghao Chen[a,b,†], Bozhi Ye[a,b,†], Diyun Xu[a,b,†], Wante Lin[a,b], Zimin Fang[a,b], Xuefeng Qu[c], Xue Han[c], Wu Luo[b], Chen Chen[a], Weijian Huang[a], Hao Zhou[a], Gaojun Wu[a], Yi Wang[b,d,*], Guang Liang[a,b,c,*]

[a]*Department of Cardiology and the Key Laboratory of Cardiovascular Disease of Wenzhou, the First Affiliated Hospital, Wenzhou Medical University, Wenzhou 325000, China*
[b]*Chemical Biology Research Center, School of Pharmaceutical Sciences, Wenzhou Medical University, Wenzhou 325035, China*
[c]*School of Pharmaceutical Sciences, Hangzhou Medical College, Hangzhou 310059, China*
[d]*School of Pharmacy, Hangzhou Normal University, Hangzhou 311121, China*

Received 28 April 2024; received in revised form 8 July 2024; accepted 26 July 2024

KEY WORDS

Deubiquitinase;
USP25;
Endothelial-to-mesenchymal transition;
Vascular remodeling;
FOXO3;
Angiotensin II;
Autolysosome;
LC3B

Abstract Long-term hypertension causes excessive vascular remodeling and leads to adverse cardiovascular events. Balance of ubiquitination and deubiquitination has been linked to several chronic conditions, including pathological vascular remodeling. In this study, we discovered that the expression of ubiquitin-specific protease 25 (USP25) is significantly up-regulated in angiotensin II (Ang II)-challenged mouse aorta. Knockout of Usp25 augments Ang II-induced vascular injury such as fibrosis and endothelial to mesenchymal transition (EndMT). Mechanistically, we found that USP25 interacts directly with Forkhead box O3 (FOXO3) and removes the K63-linked ubiquitin chain on the K258 site of FOXO3. We also showed that this USP25-mediated deubiquitination of FOXO3 increases its binding to light chain 3 beta isoform and autophagosomic-lysosomal degradation of FOXO3. In addition, we further validated the biological function of USP25 by overexpressing USP25 in the mouse aorta with AAV9 vectors. Our studies identified FOXO3 as a new substrate of USP25 and showed that USP25 may be a potential therapeutic target for excessive vascular remodeling-associated diseases.

*Corresponding authors.
E-mail addresses: wzmcliangguang@163.com (Guang Liang), yi.wang1122@wmu.edu.cn (Yi Wang).
†These authors made equal contributions to this work.
Peer review under the responsibility of Chinese Pharmaceutical Association and Institute of Materia Medica, Chinese Academy of Medical Sciences.

https://doi.org/10.1016/j.apsb.2024.12.033

1. Introduction

Aberrant and excessive remodeling of both small and large blood vessels contributes to the development and complications of hypertension[1,2]. A hallmark of this excessive remodeling is vascular fibrosis that entails the deposition of extracellular matrix in the arterial wall[3]. This increased collagen deposition is also noted in experimental models of hypertensive vascular disease[4]. Angiotensin II (Ang II) administration in mice recapitulates structural features of hypertensive vascular remodeling, including extracellular matrix deposition[5]. Studies have shown that this Ang II action is mediated in collaboration with transforming growth factor-β1 (TGF-β1)[6]. Associated with vascular fibrosis is the direct insult on endothelial cells, causing the cells to transition to a mesenchymal phenotype (EndMT)[7]. In this process, endothelial cells lose their endothelial markers such as vascular endothelial-cadherin (VE-cadherin) and induce the expression of mesenchymal genes such as *Vim*, *Snai1*, and *Snai2*[8]. EndMT has also been shown to promote vascular injury induced by Ang II and inhibition of the EndMT process by a natural product schizandrin B attenuates Ang II-induced vascular remodelling[9]. Our previous study has reported that toll-like receptor 4 mediates Ang II-induced inflammation and EndMT in vascular endothelium[10]. Therefore, it is scientifically important to identify EndMT-related regulatory molecules in the development of pathological vascular remodeling, which may provide new potential targets for the treatment of vascular remodeling-related diseases.

Recent studies link various human diseases to an imbalance in protein homeostasis mediated by ubiquitination and deubiquitination. Ubiquitination involves ubiquitin activating enzymes E1, E2, and ubiquitin ligase E3. Among these, E3 can affect the stability and activity of the substrates by linking different types of ubiquitin chains on the substrate[11]. Countering the functions of ubiquitinases are deubiquitination enzymes (DUBs), which can be divided into five families[12]: ubiquitin-specific protease (USP), ubiquitin C-terminal hydrolase (UCH), otubain protease (OTU), Machado-Joseph disease protease (MJD)/Ataxin-3, and JAB1/MPN/Mov34 metalloenzyme (JAMM). However, a thorough exploration of potential DUBs and their roles in the pathophysiology of vascular remodeling in hypertension necessitates further investigation. Since the USP family is the largest family in DUBs superfamily, we focused on the USP family and tried to identify new DUB-related mechanisms in Ang II-induced vascular remodeling. USP family has been reported to play important roles in cell signal transduction, cell fate determination, inflammation and immunity[13]. In the present study, we examined the expression levels of USP family members in Ang II-challenged mouse aortas and found that Ang II significantly increased expression of USP25. USP25, a member of the USP family, is a key target for drug development and has been reported to be involved in the development of various diseases[14,15]. Our previous study reported that USP25 alleviates pathological cardiac hypertrophy by deubiquitinating and stabilizing SERCA2[16]. However, it remains unknown whether USP25 is associated with vascular EndMT process and its role in pathological vascular remodeling is unclear.

Here, we show that Ang II-mediated EndMT and vascular fibrosis are increased in the absence of USP25. Mechanistically, we show that USP25 binds directly to FOXO3 but not other major FOXO proteins. We found cysteine 178 on USP25 is critical for the removal of K63-linked ubiquitin chain on the lysine 258 of FOXO3, and the subsequent binding of FOXO3 to autophagy-associated microtubule-associated proteins light chain 3B (LC3B) for FOXO3 degradation. The cultured endothelial cells were used to further verify that USP25 affects the development of EndMT by regulating FOXO3. In addition, restoration of USP25 in deficient mice prevents Ang II-induced pathological processes. In summary, USP25 is identified as a novel vascular endothelial cell regulatory protein that may serve as a therapeutic target for vascular remodeling-related diseases.

2. Materials and methods

2.1. General reagents

Angiotensin II (Ang II; Cat# HY-13948), 3-methyladenine (3-MA; Cat# HY-39312), chloroquine (CQ; Cat# HY-17589A), and bafilomycin A1 (Baf A1; Cat# HY-100558) were purchased from MedChemExpress (NJ, USA). Antibodies against USP25 (Cat# sc-398414) and FOXO4 (Cat# sc-373877) were purchased from Santa Cruz Biotech (TX, USA). Antibodies against SNAI1+SLUG (Cat# ab180714), VE-Cadherin (Cat# ab33168), CD31 (Cat# ab9498), Lamin B (Cat# ab133741), transforming growth factor-β1 (TGF-β1; Cat# ab179695), collagen I (Col-1; Cat# ab34710), and alpha-smooth muscle actin (α-SMA; Cat# ab7817) were obtained from Abcam (Cambridge, UK). Antibodies against GAPDH (Cat# 5174), FOXO1 (Cat# 2880), FOXO3 (Cat# 2497), and VIMENTIN (Cat# 5741) were purchased from Cell Signaling Technology (MA, USA). IgG (Cat# B900610) and antibodies against FOXO3 (Cat# 66428-1-lg), CD31 (Cat# 11265-1-AP), FOXO6 (Cat# 19122-1-AP), Flag (Cat# 20543-1-AP), HA (Cat# 51064-2-AP), His (Cat# 66005-1-lg), LAMP1 (Cat# 21997-1-AP), LAMP2 (Cat# 66301-1-lg), LC3B (Cat# 18725-1-AP) were obtained from Proteintech (Hubei, China).

2.2. Angiotensin-II induced model of vascular dysfunction

Animal experiments were initiated following approval of the animal use protocol by the Animal Policy and Welfare Committee of Wenzhou Medical University (approval ID: WYYY-AEC-YS-2022-287). All animals received humane care according to the National Institutes of Health (USA) guidelines. *Usp25* knockout mice on C57BL/6 background and the littermate wide-type C57BL/6 mice were provided by Prof. Jian Yuan of Tongji University. In the present study, heterozygous *Usp25* mice were hybridized to produce homozygous *Usp25* KO and wild-type littermate animals. The mice used in experiments are littermates. Mice were housed with a 12 h:12 h light−dark cycle at a constant room temperature and fed a standard rodent diet in a specific-pathogen-free facility. All animal experiments were performed and analyzed by blinded experimenters. Treatment groups were assigned in a randomized fashion.

To generate a hypertensive vascular dysfunction model, mice were implanted with osmotic pump (Cat# 1004; Alzet, USA) delivering saline as Sham or 1 μg/kg/min Ang II for 4 weeks. Experiments were initiated in male 8-week-old mice weighing approximately 18−22 g, randomly divided to different treatment groups. We compared WT-Sham, *Usp25*$^{-/-}$ Sham, WT-Ang II, and *Usp25*$^{-/-}$ Ang II ($n = 6$). Then, we induced the expression of *Usp25* in *Usp25*$^{-/-}$ mice by administering adeno-associated virus serotype 9 (AAV9) encoding *Usp25* (AAV9-*Usp25*; Genechem, Shanghai, China) *via* tail vein injection. Control mice received AAV9 negative vector. Mice were administered AAV9 at 2×10^{11} vg/mouse/month. Four weeks later, Ang II was infused and maintained for 4 weeks. For these studies, we compared WT-Ang II + AAV9-Vector, *Usp25*$^{-/-}$ Ang II + AAV9-Vector, *Usp25*$^{-/-}$ Ang II + AAV9-*Usp25*. At the end of the experiment, all mice were anesthetized with a 50 mg/kg dose of 1% pentobarbital sodium (Cat# P3761; Sigma−Aldrich, MO, USA) by intraperitoneal injection. Blood and aortic samples were collected. The aortas were fixed in 4% paraformaldehyde or snap-frozen in liquid nitrogen.

2.3. Histological analyses

Aortas harvested from mice were embedded in the Optimal Cutting Temperature (OCT) medium. Tissues were sectioned at 5 μm thickness and used for routine hematoxylin and eosin (H&E; Cat# G1120; Solarbio, Beijing, China) and Masson's trichrome staining (Cat# G1340; Solarbio, Beijing, China). Brightfield images were taken. Frozen tissues sections were used for immunofluorescence staining. For this, tissues were fixed in cold methanol for 10 min, permeabilized with 0.25% Triton X-100 for 10 min, and then blocked in 5% bovine serum albumin for 30 min. Primary antibodies were added and slides were kept at 4 °C overnight. Next day, primary antibody solution was removed, and slides were washed. Then, fluorophore-conjugated secondary antibodies were applied for 1 h at room temperature. Finally, anti-fluorescence quencher kit with DAPI (Cat# SP-8500-15; Vector Laboratories, USA) was used. Fluorescence images were captured using Nikon epi-fluorescence microscope (Nikon, Japan) equipped with a digital camera. For chromogen-based immunohistochemistry, slides were processed as outlined above. For detection, we used horseradish peroxidase-labeled secondary antibodies (Beyotime, Shanghai, China) for 2 h at room temperature. Diaminobenzidine (DAB) solution was then added. Slides were counterstained with hematoxylin. We used image J software to measure vessel wall thickness, the overlapping area, and the ratio of positive area for collagen and TGF-β1 in the vessel. In brief, four points (at 3, 6, 9 and 12 o'clock) were selected from the slide to measure the thickness of the vessel wall and then get the averaged data. In addition, we calculated overlapping areas and the ratio of positive area for collagen and TGF-β1 in vessels using the "Threshold" tool in this software.

2.4. Transcriptome sequencing

Total RNA from aortas was isolated using RNAiso Plus (Cat# 9108; Takara, Japan). Samples were sent to LC-Bio (Hangzhou, China) for genome-wide transcriptome analysis. Differentially expressed genes with a fold change > 2 or fold change < 0.5 were selected with a P value < 0.05. Gene set enrichment analysis of signaling pathways (GSEA, https://www.gsea-msigdb.org/gsea/index.jsp) was performed by LC-Bio (https://www.lc-bio.cn/).

2.5. Cell culture studies

Murine aortic endothelial cells (MAECs) were isolated as reported previously[17]. Briefly, we first removed the aorta from C57BL/6 mice, quickly removed the perivascular adipose tissue and connective tissue, and cut the aorta into 1 mm vascular rings. Subsequently, we cut the vascular ring open with ophthalmic scissors and placed it endothelium down on a 6-well culture plate pre-coated with growth factor reduced matrigel (Cat# 0827035; ABW, Shanghai, China). Tissues were cultured in endothelial cell culture medium (Cat# 1001; ScienCell, USA) supplemented with 1% endothelial cell growth supplement, 5% fetal bovine serum (FBS), and 1% penicillin/streptomycin. After 5−7 days, vascular networks were visible under the light microscope and tissue segments were removed. We then removed the tissue sections and continued to culture MAECs for 3 days. Cells were passaged onto new culture plates without Matrigel and used for studies.

Murine aortic smooth muscle cells (MASMCs) were isolated as reported previously[18]. Briefly, we first removed a 5 mm segment of C57BL/6 mouse aorta. Then, we removed the adventitia and cut open with ophthalmic scissors. The endothelium was scraped with curved forceps to remove the endothelium. The vascular tissue was cut into pieces and transferred to culture dishes for 7−10 days. MASMCs were cultured in a DMEM/F12 medium (Cat# C11330500BT; GIBCO, Germany) supplemented with 20% FBS and 1% penicillin/streptomycin. Cells were passaged onto new culture plates and used for studies.

Human umbilical vein endothelial cells (HUVECs), HEK-293T, and NIH/3T3 cells were purchased from the Shanghai Institute of Biochemistry and Cell Biology (Shanghai, China). A DMEM medium (Cat# C11995500BT; GIBCO, Germany) with 4.5 g/L glucose containing 10% FBS and 1% penicillin/streptomycin was used to culture the cells. Human vascular adventitial fibroblasts (HVAFs) and Human vascular smooth muscle cells (HVSMCs) were obtained from Pricella Life Science & Technology Co., Ltd. (Wuhan, China). All cells were placed in a humidified incubator with 5% CO_2 and 37 °C temperature.

Expression of wildtype *Usp25* and various other constructs was achieved by transfecting cells with plasmids using LipofectAMINE 3000 (Cat# L3000015; Invitrogen, USA). Plasmids were obtained from Genechem and included: Flag-USP25, Flag-mut-USP25, Flag-USP25-C178A, Flag-USP25-H608A, His-FOXO3, His-FOXO3-K258R, HA-Ub, HA-K48, and HA-K63. To knockdown the expression of *Usp25*, *Lamp2*, and *Lc3b*, cells were transfected with si-USP25 (human, GCCAGUGCAUACUGUUUAATT; mouse, GCCTCCATCAAATGCTCAA), si-LAMP2 (mouse, GCA GAATGGGAGATGAATT), si-LC3B (mouse, CCCAGTGAT TATAGAGCGA), respectively (Ribobio, Guangzhou, China). Scrambled sequences were used as the negative control.

2.6. Usp25 knockout in NIH/3T3 cells

HEK-293T and NIH/3T3 cells were procured from the Shanghai Institute of Biochemistry and Cell Biology (Shanghai, China). We cloned gRNA targeting the mouse *Usp25* gene into lenticas9-blast plasmid (Cat# 52962; Addgene, USA). gRNA sequence is shown in Supporting Information Table S1. Pspax2, Pmd2.g, and lentiCas9-Blast-USP25 gRNA were then co-transfected into HEK-293T cells. Cells were cultured for 48 h, and the supernatant was collected to obtain lentivirus. We then infected NIH/3T3 fibroblasts and selected monoclonal cell lines by the blast method.

Expression of USP25 was verified by immunoblotting. *Usp25* deficient cell lines were selected.

2.7. Coimmunoprecipitation assay

Lysates from tissues or cells were prepared. Primary precipitating antibody was added to the samples. Samples were incubated overnight on a shaker. The next day, agarose magnetic beads were added to the samples and incubated for 6 h. Then, samples were centrifuged, and supernatants removed. After cleaning the beads, the process was repeated 5 times. Samples were boiled and used for immunoblotting.

2.8. Western blot

Cell and tissue lysates were prepared in RIPA buffer (Cat# P0013B; Beyotime Biological Technology, Shanghai, China) and protein concentration was measured. Protein lysates were separated by sodium dodecyl sulfate-polyacrylamide gel electrophoresis and transferred to polyvinylidene fluoride membranes. Membranes were blocked in Tris-buffered saline (pH 7.4, containing 0.05% Tween 20 and 5% non-fat milk) for 1 h at room temperature and incubated with primary antibodies at 4 °C overnight. Secondary antibodies were applied for 1 h at room temperature. Immunoreactivity was visualized using enhanced chemiluminescence reagent (Bio-Rad) and quantified using Image J analysis software version 1.53. Values were normalized to respective housekeeping proteins.

2.9. In vitro ubiquitination assay

Usp25 knockout NIH/3T3T cells were transfected with Flag, Flag-USP25, or His-FOXO3, plus HA-K48/K63 Ub plasmids. Immunoprecipitation was used to collect Flag-USP25 and K48/K63 ubiquitinated FOXO3 from cell lysates were detected. PBS and deubiquitination buffer (50 mmol/L Tris−HCl, 5 mmol/L $MgCl_2$, 2 mmol/L DTT, 2 mmol/L ATP-Na_2, 5% glycerol) were used to wash immunoprecipitated samples. The ubiquitinated FOXO3 was then incubated with Flag or Flag-USP25 in the deubiquitination buffer for 2 h at 37 °C, followed by Western blot analysis.

2.10. Prediction of ubiquitinated lysine sites in FOXO3

We used the UbiqSite (http://systbio.cau.edu.cn/ubiqsite/) and GPS-Uber (http://gpsuber.biocuckoo.cn/online.php) for prediction of ubiquitination sites on FOXO3. The top three scoring lysine sites in the results were selected for analysis.

2.11. Real-time quantitative polymerase chain reaction (PCR)

Total RNA from samples was isolated using Trizol (Cat# 15596026; Thermo Fisher, USA). RNA was reverse-transcribed using PrimeScript RT reagent (Cat# RR047A; Takara, Japan). Real-time PCR was subsequently conducted using TB Green Premix Ex Taq II (Cat# RR820A; Takara, Japan) on QuantStudio RT PCR (Applied Biosystems, USA). Relative expression was calculated by $2^{\Delta\Delta Ct}$ method with *Actb* normalization. Primer sequences used for qPCR are listed in Supporting Information Table S2.

2.12. Immunogold electron microscopy

We quickly removed 1 mm of mouse aortic tissue and placed it in a fixative, followed by alcohol dehydration, resin infiltration and embedding of the sample. The 70−80 nm of slices was immunolabelled with FOXO3 and immunogold antibodies, and finally placed under a transmission electron microscope for observation and image recording.

2.13. Cleavage under targets and tagmentation (CUT&Tag) assay

We performed CUT&Tag assay using the NovoNGS CUT&Tag 3.0 High-Sensitivity Kit (N259-YH01, Novoprotein, China) according to the instructions. In brief, cells were first collected in 90 μL wash buffer and mixed with 10 μL ConA beads for 10 min at room temperature (RT). Subsequently, the cell samples were treated with anti-FOXO3 antibody for 2 h and incubated with secondary antibody for 1 h. Transposome pA-Tn5 was then introduced and incubated with the cell samples for 1 h. DNA fragments were isolated using Tagment DNA extraction beads and dissolved in 37 μL TE buffer. The DNA was amplified using the corresponding primers and subjected to qPCR analysis. Promoter primer sequences are shown in Supporting Information Table S2.

2.14. Statistical analysis

All experiments were randomized and blinded. The data presented in this study represent at least 3 independent experiments and presented as mean ± standard error of mean (SEM). For *in vitro* experiments, given that the values obtained for each experiment were the average of a large number of cultured cells, we assumed that the data were normally distributed according to the central limit theorem. For the analysis of the *in vivo* experiments, since our sample size equals 6, we first assessed the normality of the distribution of each data using the Shapiro−Wilk test. $P > 0.05$ indicated that the data in each group were approximately normally distributed. Comparisons between two groups were analyzed using Student's *t* test. When comparing data from more than two groups, we used one-way ANOVA followed by Tukey's *post hoc* test. $P < 0.05$ was considered statistically significant. Statistical analysis was performed with GraphPad Prism 8.0 software (San Diego, CA, USA).

3. Results

3.1. Usp25 deletion aggravates vascular remodeling in Ang II-challenged mice

To explore the potential relevance of DUBs in vascular remodeling, we used an experimental model of chronic Ang II challenge. Mice were administered Ang II for 4 weeks and aortas were harvested. This 4-week Ang II infusion model in mice has been reported to successfully induce aortas EndMT and remodeling[19]. RNA sequencing of mouse aortas showed changes in the gene expression of USP family members (Fig. 1A). We selected the top 10 USPs that appeared to be most upregulated and performed real-time qPCR validation. From this, we identified *Usp25* as significantly increased in aortas of mice challenged with Ang II (Fig. 1B). We also observed similar results for USP25 at the protein level (Fig. 1C and D), indicating a relevance of USP25 in this model. To investigate this potential role of USP25 in our

system, we utilized *Usp25* knockout mice. These mice showed no detectable levels of USP25 in the aorta (Supporting Information Fig. S1), providing an appropriate experimental platform to investigate the function. We administered Ang II in both wildtype and *Usp25*$^{-/-}$ mice for 4 weeks and examined the blood pressure. The results showed that *Usp25* knockout did not affect blood pressure profiles in both Sham and Ang II-infused mice (Supporting Information Fig. S2). Hematoxylin and eosin (H&E) staining of the aortas showed clear signs of excessive vascular remodeling in Ang II-administered mice. Interestingly, *Usp25* knockout mice showed more pronounced histopathological features of vessel wall thickening compared to wildtype mice (Fig. 1E−G). As the process of vascular remodeling is often accompanied by excessive collagen deposition[4], we then stained the tissues with Masson's trichrome. The outcomes confirmed that *Usp25* knockout mice exhibit increased vascular fibrosis upon Ang II challenge (Fig. 1H and I). TGF-β1 immunoreactivity paralleled Masson Trichrome staining (Fig. 1J and K), showing that Ang II causes more TGF-β1 expression in *Usp25* knockout mice compared to wildtype mice. Notably, in the absence of Ang II stimulation, no significant histopathological changes were observed in the aorta of *Usp25* knockout mice compared to the WT mice. Collectively, we found that *Usp25* deficiency exacerbated Ang II-induced vascular remodeling.

3.2. *Usp25 deletion promoting endothelial EndMT in Ang II-challenged mouse aortas*

To further investigate the regulatory role of USP25 on vascular remodeling, we isolated primary aortic endothelial and primary smooth muscle cells separately and stimulated them with Ang II. Surprisingly, isolated murine aortic endothelial cells (MAECs) showed a time-dependent increase in USP25 upon Ang II exposure (Fig. 2A and B). However, this phenomenon was not observed in murine aortic smooth muscle cells (MASMCs) (Fig. 2C and D). We performed immunofluorescence assay to examine the USP25 distribution in vascular tissues of mice with or without Ang II infusion. The results showed that the basal level of USP25 in CD31^{+} endothelial cells was much higher than α-SMA^{+} smooth muscle cells and VIMENTIN^{+} fibroblasts in the control mice. Notably, USP25 was significantly elevated in endothelial cells but not in fibroblasts and smooth muscle cells after Ang II challenge (Supporting Information Fig. S3A−S3C). Endothelial cells, vascular fibroblasts, and vascular smooth muscle cells are involved in the regulation of vascular remodeling and vascular fibrosis[20-23]. We then utilized three human-derived cells to examine the USP25 expression. Western blot assay showed that USP25 expression level in HUVECs was significantly increased after Ang II challenge, whereas no significant changes in USP25 levels were observed in HVSMCs and HVAFs (Fig. S3D). These results indicate that vascular endothelial cells are the main source of up-regulated USP25 in Ang II-induced arterial remodeling.

Subsequently, we examined the effects of *Usp25* knockdown on the function of three types of cells by qPCR. The results showed that USP25 significantly exacerbated Ang II-induced EndMT and fibrosis in HUVECs (Supporting Information Fig. S4A), but had no significant effect on the function of HVAFs and HVSMCs (Supporting Information Fig. S4B and S4C). These results indicate that *Usp25* knockout-mediated exacerbation of vascular remodeling is mainly due to excessive EndMT in endothelial cells. To further validate the effect of USP25 on EndMT in *in vivo* experiments, we stained the aortas of mice with CD31, together with VE-cadherin, VIMENTIN, or SNAI1/SLUG (Fig. 2E−J; Supporting Information Fig. S5). We found that Ang II administration increases mesenchymal phenotype-associated markers (VIMENTIN, SNAIl, and SLUG) immunoreactivity and decreases endothelial phenotype-associated markers (VE-cadherin) in CD31-positive endothelial cells in aortic tissues from Ang II-challenged mice. As expected, *Usp25* deficiency appeared to amplify these pathological changes. These data collectively show that *Usp25* deficiency exacerbated Ang II-induced endothelial EndMT.

3.3. *USP25 interacts with FOXO3 through the USP domain*

To understand the function of USP25 in Ang II-mediated vascular changes, we profiled vascular mRNA from wildtype and *Usp25* knockout mice administered Ang II. A large number of changed genes were identified (Fig. 3A). Interestingly, GSEA analysis indicated changes in the FOXO signaling pathway (Fig. 3B), which has been reported to regulate vascular remodeling and EndMT[24]. We then screened for genes involved in EndMT and show that *Usp25* deficiency is associated with excessive Ang II-induced EndMT processes (Fig. 3C). In addition, Fig. 3C also showed the *Usp25* deficiency-induced changes of FOXO-targeted genes, further validating the effect of USP25 on the FOXO signaling pathway.

Since DUBs primarily carry out their function by binding to their targets, we explored the possibility that USP25 may regulate FOXO proteins *via* direct interaction. Commonly, FOXO family contains 4 members, FOXO1, 3, 4, and 6. We prepared lysates from Ang II-challenged aortas of wildtype mice and immunoprecipitated USP25. Interestingly, immunoblotting showed interaction of USP25 only with FOXO3 (Fig. 3D). Other FOXO proteins screened did not show detectable levels, indicating that USP25 may specifically bind to FOXO3. To confirm these results, we knocked out *Usp25* by CRISPR/Cas9 in NIH/3T3 cells. We then transfected these cells with Flag-USP25 and His-FOXO3. Using this model, we validated that USP25 directly associates with FOXO3 (Fig. 3E). In addition, immunoprecipitation of USP25 in MAECs exposed to Ang II also confirmed this interaction of USP25 with FOXO3 (Fig. 3F). We further determined the key domains in USP25 and FOXO3 proteins for USP25−FOXO3 interaction. USP25 has four domains: a ubiquitin-associated domain (UBA), two tandem ubiquitin-interacting motifs (UIMs), and a ubiquitin-specific protease domain (USP). We constructed four different USP25 mutants (Fig. 3G) and transfected these in *Usp25*$^{-/-}$ NIH/3T3 cells. We showed that USP25 was unable to bind FOXO3 when amino acids 169 to 658 were missing (Fig. 3H). Using a similar method, we showed that the FOXO3−USP25 interaction disappeared when FOXO3 lost its KIX domain, suggesting that FOXO3 interacts with USP25 through the KIX domain (Supporting Information Fig. S6). These findings collectively demonstrated that USP25 binds to FOXO3 through the USP domain and KIX domain, respectively.

3.4. *USP25 promotes autophagic degradation of FOXO3*

Deubiquitinating enzymes tend to influence their downstream biological processes by regulating substrate protein stability or activity. Therefore, we first examined the protein level of FOXO3 in the aortic tissues of Ang II-challenged WT and *Usp25* knockout mice and found that FOXO3 is increased in *Usp25* knockout mice (Fig. 4A and B). However, no significant difference was found in

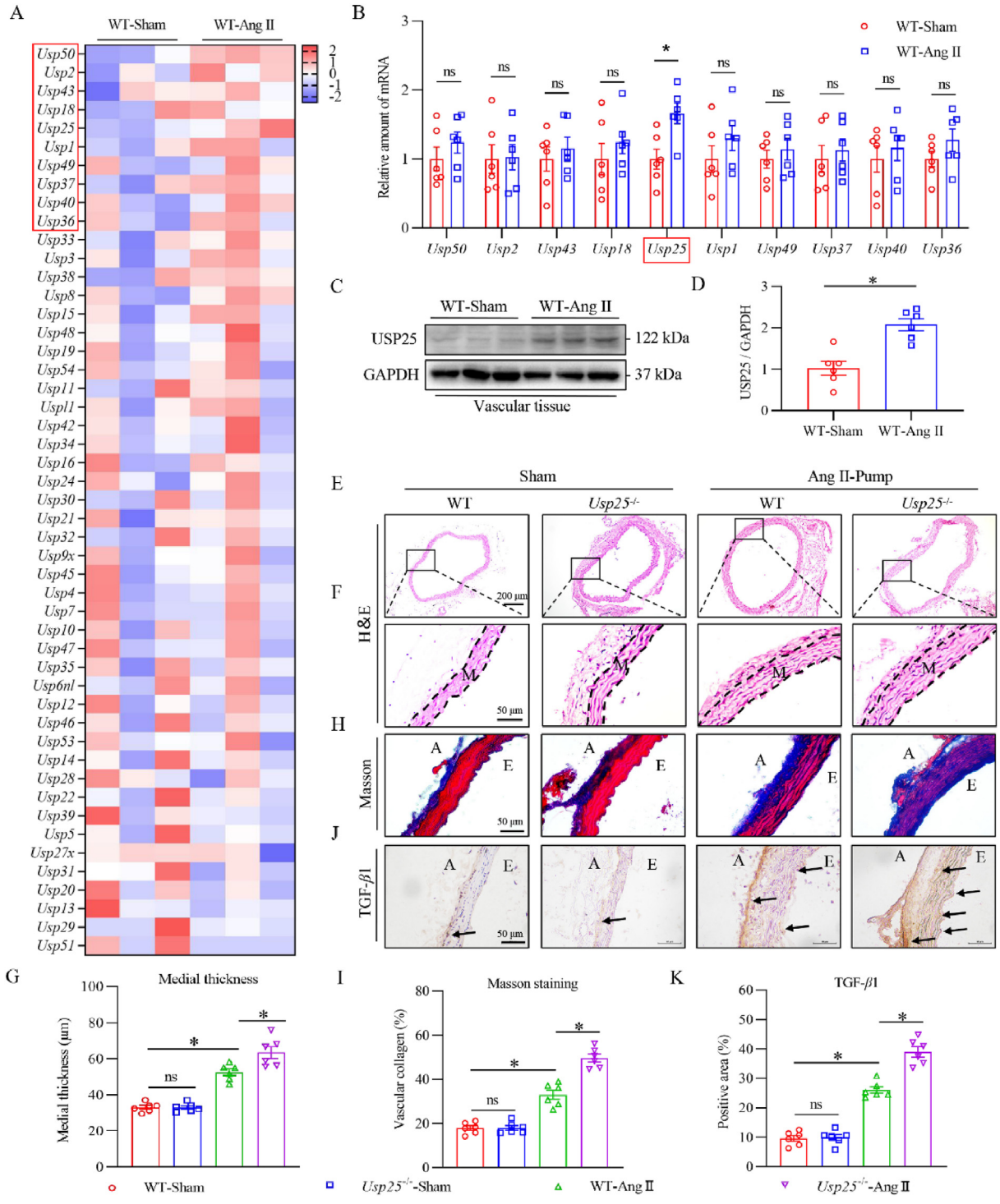

Figure 1 *Usp25* deletion aggravates vascular remodeling in Ang II-challenged mice. (A, B) Wildtype C57BL/6 (WT) mice were infused with Ang II for 4 weeks. Control (sham) mice received saline. Aortas were harvested and RNA sequencing was performed. Figure showing a heat map of deubiquitinating enzymes in the USP family ($n = 3$). Top upregulated *Usp* genes are highlighted in the red box (A). mRNA levels of the top 10 upregulated *Usp* genes as determined by qPCR (B). Data was normalized to *Actb* (mean ± SEM; $n = 6$; ns = not significant, $^*P < 0.05$). (C, D) Wildtype C57BL/6 (WT) mice were infused with Ang II for 4 weeks. Control (sham) mice received saline. Lysates from aortas were probed for FOXO3 and USP25 proteins by Western blot assay (C). GAPDH was used as the loading control. Densitometric quantification of USP25 is shown in (D) (mean ± SEM; $n = 6$; ns = not significant, $^*P < 0.05$). (E, F) Wildtype C57BL/6 (WT), and $Usp25^{-/-}$ mice were infused with Ang II for 4 weeks. Control (sham) mice received saline. Aortas were harvested and examined. Representative low-power (E) and high-power (F) images of H&E-stained aortas from mice (scale bar = 200 μm in panel (E) and 50 μm in panel (F); M = media). (G) Quantification of medial thickness in mice determined from H&E-stained sections (mean ± SEM; $n = 6$; ns = not significant, $^*P < 0.05$). (H, I) Aortic tissues were stained with Masson's trichrome to mark fibrosis. Representative staining images are shown in panel (H) (Scale bar = 50 μm; E = endothelium, A = adventitia). Quantification of

the mRNA level of *Foxo3* (Fig. 4C). To confirm this inverse relationship between USP25 and FOXO3, we transfected different amounts of Flag-USP25 in both *Usp25*$^{-/-}$ NIH/3T3 and HUVECs cells. The results showed that sequential decrease in FOXO3 as USP25 increased (Fig. 4D and E; Supporting Information Fig. S7A and S7B). Again, mRNA levels of *Foxo3* were not found to be altered (Fig. 4F; Fig. S7C). The results suggest that USP25 regulates the post-translational modification of FOXO3 and negatively affects the protein stability of FOXO3.

We next examined proteasomal and autophagic lysosomal pathway in regulating FOXO3 stability downstream of USP25. We expressed USP25 in *Usp25*$^{-/-}$ NIH/3T3 cells and exposed the cells to various proteasomal or lysosomal inhibitors. These inhibitors included proteasomal inhibitor MG132, and autophagy inhibitors 3-methyladenine (3-MA), chloroquine (CQ), and bafilomycin A1 (Baf A1). We show that MG132 had no significant effect on the USP25-mediated degradation of FOXO3, while autophagy inhibitors reversed this USP25-induced FOXO3 degradation (Supporting Information Fig. S8; Fig. 4G). In addition, treatment of mice with 3-MA also reversed USP25 overexpression-induced FOXO3 degradation in Ang II-challenged mouse aortas (Supporting Information Fig. S9). Knockdown of *Usp25* also reduced Ang II-stimulated autophagic flux in endothelial cells (Supporting Information Fig. S10). Next, we expressed USP25 and FOXO3 in *Usp25*$^{-/-}$ NIH/3T3 cells and exposed the cells to Earle's balanced salt solution (EBSS) to induce autophagy. Autophagic degradation of FOXO3 is accelerated in EBSS-exposed cells when USP25 is expressed (Fig. 4H and I). These results suggest that USP25 mediates the degradation of FOXO3 mainly through the autophagic pathway. Moreover, FOXO3 significantly co-localized with the lysosome marker LAMP1 (Supporting Information Fig. S11A). The co-localization of USP25 and LAMP1 was significantly increased after Ang II treatment and was further enhanced upon overexpression of USP25 in HUVECs (Fig. S11B). Immunogold electron microscopy results further showed that FOXO3 was located in the autophagic lysosomes of WT mouse endothelial cells, while disappeared in the autophagic lysosomes of *Usp25*$^{-/-}$ endothelial cells, indicating that USP25 promotes the autophagic translocation and degradation of FOXO3 (Fig. S11C). Chaperone-mediated autophagy is also an important mode of autophagic degradation, mediated mainly through LAMP2[25]. However, we found that silencing LAMP2 did not inhibit the USP25-induced degradation of FOXO3, indicating that the autophagic degradation of FOXO3 is independent of chaperone (Supporting Information Fig. S12).

To identify the active site on USP25 in regulating FOXO3, we transfected *Usp25*$^{-/-}$ NIH/3T3 cells with Flag-USP25-C178A or Flag-USP25-H608A (Supporting Information Fig. S13), based on previous studies[26], and examined FOXO3 expression. We showed that the expression of wildtype USP25 and USP25−H608A both reduced FOXO3 protein levels (Fig. 4J). USP25−C178A, however, did not change FOXO3 proteins. Similarly, under EBSS exposure, we observed that USP25−C178A did not accelerate the autophagic degradation of FOXO3 (Fig. 4K and L). These results suggest that the cysteine at position 178 in USP25 plays a role in the degradation of FOXO3.

3.5. FOXO3 interacts with LC3B

We then examined whether USP25 affects FOXO3 binding to key autophagic proteins. Transfection of *Usp25*$^{-/-}$ NIH/3T3 cells with His-FOXO3 and one of P62 or LC3B autophagy-associated proteins showed that FOXO3 binds to LC3B but not P62 (Fig. 4M and N). Immunofluorescence assay showed the co-location of FOXO3 and LC3B (Supporting Information Fig. S14A). Ang II treatment enhanced the co-localization between the FOXO3 and LC3B, which was further increased by the transfection of USP25 plasmid in both NIH/3T3 and HUVEC cells (Fig. 4O; Fig. S14B and S14C). However, FOXO3 and P62 still did not bind when overexpressing USP25 (Supporting Information Fig. S15). Moreover, after silencing LC3B, USP25 was no longer able to significantly degrade FOXO3 (Supporting Information Fig. S16). Three autophagy inhibitors CQ, Baf A1, and 3-MA were used to further examine the autophagic degradation and LC3B interaction of FOXO3. NIH/3T3 cells transfected with Flag-USP25 were treated with these inhibitors, respectively. The results of immunofluorescence staining showed that the levels of FOXO3 increased after treatment of three autophagy inhibitors. Interestingly, the co-localization of FOXO3 with LC3B seems to be different among the three inhibitor-treated groups. Only 3-MA treatment decreased the FOXO3−LC3B interaction, suggesting that the binding of FOXO3 to LC3B occurs at an early stage of autophagosome formation (Supporting Information Fig. S17). These results show that USP25 increases FOXO3 degradation through the LC3B-mediated autophagic lysosomal pathway.

3.6. USP25 reverses K63-linked ubiquitination of lysine 258 on FOXO3

K48 and K63 are the classical ubiquitin chain types but often mediate different effects. We investigated the effect of USP25 on K48, K63, and total ubiquitin on FOXO3 proteins. We found that USP25 removes the K63 ubiquitin chain on FOXO3 protein, without affecting the K48 ubiquitin chain in NIH/3T3 cells (Fig. 5A−C). A similar result was observed in HUVECs (Supporting Information Fig. S18). This result was confirmed by *in vitro* deubiquitinating assays using the extracted proteins (Fig. 5D−F). Mutating C178 on USP25 prevents the removal of the K63 ubiquitin chain on FOXO3 while USP25−H608A retains the ability (Fig. 5G). Finally, we explored which lysine sites on FOXO3 are affected by USP25. We predicted the ubiquitination sites on FOXO3 using two databases: UbiqSite and GPS-Uber (Fig. 5H and I). Lysine at position 258 of FOXO3 represented the intersection of the two. We, therefore, constructed the corresponding FOXO3-K258R mutant plasmid. Expression of this mutant FOXO3 with USP25 showed that USP25 no longer had a significant effect on the K63 ubiquitin chain of FOXO3 (Fig. 5J), despite that the FOXO3-K258R still interact with USP25 protein (Supporting Information Fig. S19). As expected, USP25 showed no significant effect on the degradation curve of FOXO3-K258R (Supporting Information Fig. S20). Interestingly, we found that the K258R mutation also significantly reduced the interaction of FOXO3 with LC3B (Supporting Information Fig. S21). In summary, we show that USP25 removes the K63-linked ubiquitin chain from the lysine at position 258 of FOXO3.

collagen from Masson's trichrome-stained sections is shown in panel (I) (mean ± SEM; $n = 6$; ns = not significant, $^*P < 0.05$). (J, K) Representative immunohistochemical staining for TGF-β1 (brown) in aortas are shown in panel (J) (Scale bar = 50 μm; E = endothelium, A = adventitia). Quantification of the positive area from immunohistochemical sections of TGF-β1 is shown in panel (K) (mean ± SEM; $n = 6$; ns = not significant, $^*P < 0.05$). Student's *t*-test (unpaired, two-tailed) for (B, D). One-way ANOVA followed by Tukey *post hoc* test for (G, I, K).

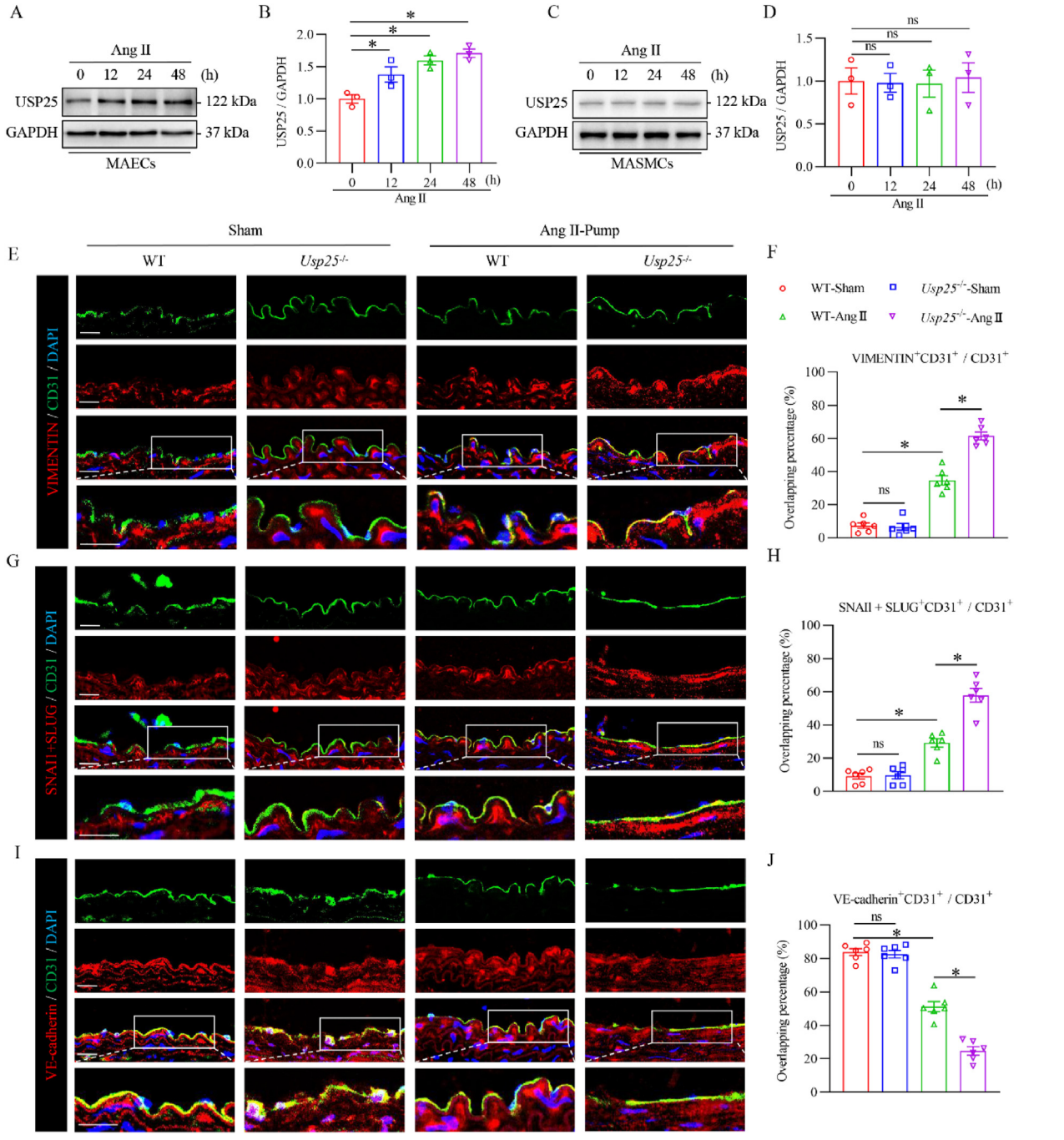

Figure 2 *Usp25* deletion promoting aortic EndMT in Ang II-challenged mice. (A, B) Murine aortic endothelial cells (MAECs) were exposed to 1 μmol/L Ang II for different time periods. Lysates were probed for USP25 (A). GAPDH was used as the loading control. Densitometric quantification of USP25 is shown in (B) (mean ± SEM; $n = 3$; ns = not significant, $^*P < 0.05$). (C, D) Murine aortic smooth muscle cells (MASMCs) were exposed to 1 μmol/L Ang II for different time periods. Lysates were probed for USP25 (C). GAPDH was used as the loading control. Densitometric quantification of USP25 is shown in (D) (mean ± SEM; $n = 3$; ns = not significant, $^*P < 0.05$). (E, F) Representative double immunofluorescence staining images showing expression of VIMENTIN (red) and CD31 (green) in panel (E). Sections were counterstained with DAPI (blue). Proportion of overlapping area is shown in (F) (Scale bar = 20 μm). (G, H) Representative double immunofluorescence staining images showing expression of SNAI1+SLUG (red) and CD31 (green) in panel (G). Sections were counterstained with DAPI (blue). Proportion of overlapping area is shown in (H) (Scale bar = 20 μm). (I, J) Representative double immunofluorescence staining images showing expression of VE-cadherin (red) and CD31 (green) in panel (I). Sections were counterstained with DAPI (blue). Proportion of overlapping area is shown in (J) (Scale bar = 20 μm). One-way ANOVA followed by Tukey's *post hoc* test for (B, D, F, H, J).

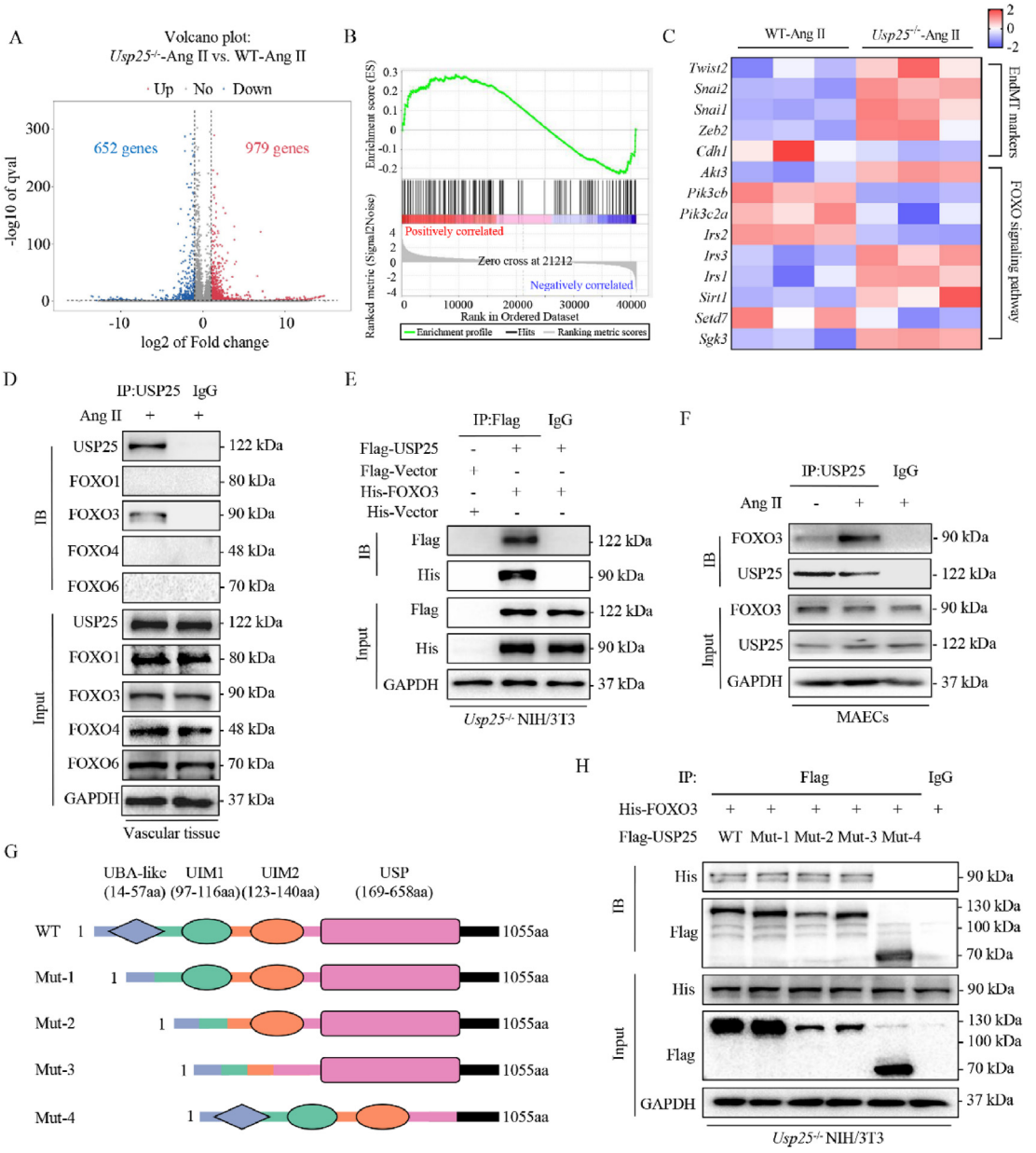

Figure 3 USP25 interacts with FOXO3 through the USP domain. (A–C) Total aortic RNA from wildtype and *Usp25*$^{-/-}$ mice challenged with Ang II for 4 weeks was sequenced. Figure showing a volcano plot (A), GSEA analysis of FOXO pathway (B), and a heat map (C) of genes involved in EndMT and FOXO signaling pathway ($n = 3$). (D) Mouse aortic tissue lysates from Ang II-challenged wildtype mice were immunoprecipitated with USP25 antibody. Levels of FOXO3 were determined by immunoblotting. IgG was used as the control for IP. (E) *Usp25* was knocked out in NIH/3T3 cells by CRISPR/Cas9. Cells were then transfected with Flag and His vectors or Flag-USP25 and His-FOXO3. Flag was immunoprecipitated. IgG was used as the control. Interaction between USP25 and FOXO3 was detected by immunoblotting. (F) MAECs were exposed to 1 μmol/L Ang II for 48 h or not. USP25 was immunoprecipitated and FOXO proteins were detected by immunoblotting. IgG was used as the control for immunoprecipitation. Lysates prior to immunoprecipitation were used as input. (G) Schematic showing the structure of wildtype USP25 and various mutants [pink = USP domain; orange and green circles = Ubiquitin-interacting motifs (UIMs), blue = ubiquitin-associated domains (UBAs)]. (H) *Usp25*$^{-/-}$ NIH/3T3 cells were transfected with His-FOXO3 and either Flag-wildtype USP25 or one of the mutants. Anti-flag was used for immunoprecipitation. His-tagged FOXO3 was determined by immunoblotting. IgG was used as the control for IP.

3.7. USP25 impacts EndMT by regulating FOXO3 in endothelial cells

FOXO3 has been reported as a cofactor for the transcriptional activity of the TGF–Smad pathway, a regulator of EndMT[27]. To explore how USP25–FOXO3 dynamics play a role in EndMT, we first examined the effect of USP25 on FOXO3 content in endothelial cells. We transfected MAECs with USP25 expression vector and exposed the cells to Ang II. Our results showed that USP25 significantly reduced the protein levels of FOXO3 in the nucleus and cytoplasm (Fig. 6A). Subsequently, we silenced *Usp25* using siRNA and showed that *Usp25* knockdown increased

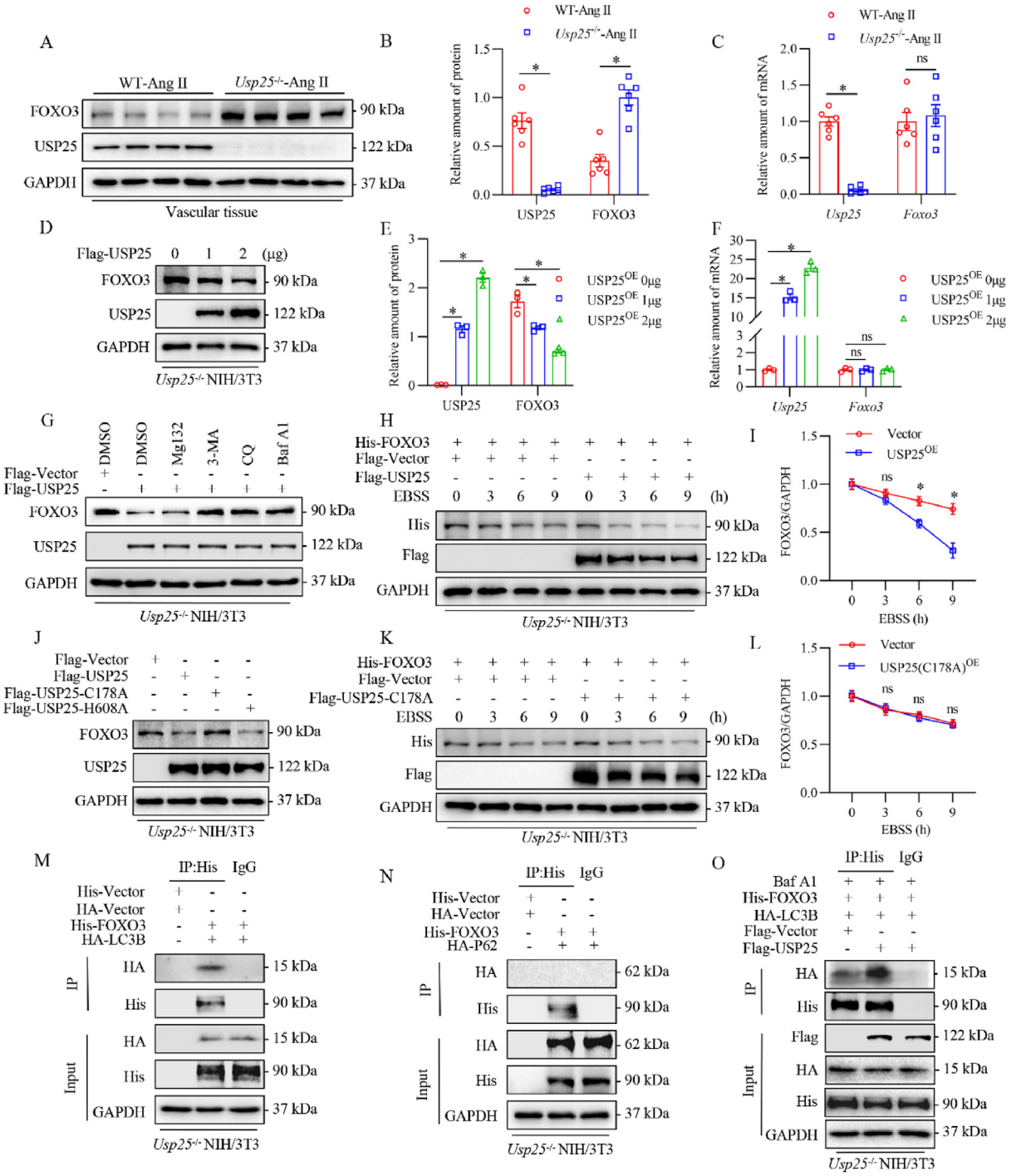

Figure 4 USP25 promotes FOXO3 degradation by enhancing FOXO3−LC3B interaction. (A) Wildtype and *Usp25*$^{-/-}$ mice were challenged with Ang II for 4 weeks. Lysates from aortas were probed for FOXO3 and USP25 proteins. GAPDH was used as the loading control. (B) Densitometric quantification of USP25 and FOXO3 from Panel (A) (mean ± SEM; $n = 3$; *$P < 0.05$). (C) mRNA levels of *Usp25* and *Foxo3* in aortic tissues of wildtype and *Usp25*$^{-/-}$ mice challenged with Ang II. Data was normalized to *Actb* (mean ± SEM; $n = 6$; ns = not significant, *$P < 0.05$). (D) *Usp25*$^{-/-}$ NIH/3T3 cells were transfected with Flag-USP25. Levels of FOXO3 and USP25 proteins were determined. (E) Densitometric quantification of USP25 and FOXO3 from Panel (D) (mean ± SEM; $n = 3$; *$P < 0.05$). (F) mRNA levels of *Usp25* and *Foxo3* in *Usp25*$^{-/-}$ NIH/3T3 cells transfected with Flag-USP25. Data was normalized to *Actb* (mean ± SEM; $n = 3$; ns = not significant, *$P < 0.05$). (G) *Usp25*$^{-/-}$ NIH/3T3 cells were transfected with Flag-USP25 or Flag-vector. Cells were then treated with 10 μmol/L MG132, 10 mmol/L 3-methyladenine (3-MA), 50 μmol/L chloroquine (CQ), or 0.2 μmol/L bafilomycin A1 (Baf A1) for 6 h. Lysates were probed for USP25 and FOXO3. GAPDH was used as the loading control. (H) *Usp25*$^{-/-}$ NIH/3T3 cells transfected with Flag-USP25 and His-FOXO3 were cultured in Earle's balanced salt solution (EBSS) for various time points. Flag-vector transfected cells were used as the control. Lysates were probed for His (FOXO3) and Flag (USP25). GAPDH was used as the loading control. (I) Densitometric quantification of FOXO3 from Panel (H) (mean ± SEM;

Ang II-induced expression of SNAI1, SLUG, VIMENTIN, COL1A1, and TGF-β1, and decreased the expression of VE-cadherin, while overexpression of *Usp25* maintained VE-cadherin and reduced mesenchymal cell-associated and fibrosis-associated proteins following Ang II exposure (Fig. 6B and C; Supporting Information Fig. S22). These results were confirmed at the mRNA level (Fig. 6D). Interestingly, we found that FOXO3 expression could reverse the effect of USP25 overexpression on Ang II-induced EndMT (Fig. 6E−G). Next, we explored how FOXO3 regulated the transcription of EndMT-related genes in HUVECs with or without USP25 overexpression using CUT&Tag assay. Our results showed that FOXO3 can bind to the promoter regions of *SANI1*, *SNAI2*, and *VIM* genes in HUVECs, and the enrichments of FOXO3 were significantly decreased when over-expressing USP25. These results demonstrate that FOXO3 directly up-regulates the transcription of EndMT-related genes and USP25 inhibits these gene transcriptions *via* reducing the FOXO3 level (Supporting Information Fig. S23). The above results indicated that USP25 regulates the Ang II-induced EndMT by regulating FOXO3-mediated transcription of EndMT-related genes.

3.8. *USP25 induction suppresses Ang II-induced vascular remodeling*

Gene therapy based on adeno-associated virus (AAV) vector has been applied to clinical treatment[28]. To explore the effects of restoring USP25 in vascular remodeling, we constructed AAV9-*Usp25* and administered to *Usp25*-deficient mice by tail vein injection. This system increased USP25 expression in the aortas of *Usp25*-deficient mice (Supporting Information Fig. S24). We then challenged these mice with Ang II and examined the outcome. H&E staining of aortas showed that restoration of USP25 in *Usp25*-deficient mice suppresses Ang II-induced aortic vessel wall histopathology and thickening (Fig. 7A−C). Masson's trichrome staining and TGF-β1 immunoreactivity staining also showed that restoration of USP25 plays a protective role in Ang II-induced fibrotic changes (Fig. 7D−G). Immunofluorescence staining of the aortas showed that restoration of USP25 reduces the level of aortic endothelial cells expressing EndMT markers upon Ang II administration (Fig. 7H−M; Supporting Information Fig. S25). These results show that restoration of USP25 in mice suppressed Ang II-induced endothelial EndMT as well as vascular remodeling.

4. Discussion

In this study, we identified *Usp25* as a significantly upregulated DUB in aortas of mice challenged with Ang II. Surprisingly, *Usp25* deficiency increased the deleterious response to Ang II in mice, and restoration of USP25 expression in deficient mice dampened excessive vascular remodeling. Mechanistically, we found that the USP domain of USP25 can directly bind FOXO3, which facilitates the binding of FOXO3 to LC3B and promotes autophagosome−lysosomal degradation of FOXO3. The critical role of USP25 in this process relates to USP25 cysteine 178 in removing the K63-linked ubiquitin chain on the lysine 258 of FOXO3. A schematic summary of the major findings is presented in the graphic abstract.

Deubiquitinating enzymes are emerging as important players in the regulation of vascular remodeling. Our group previously reported that endothelial OTUD1 promotes Ang II-induced vascular remodeling through deubiquitination of SMAD3[19]. An et al. showed that a novel deubiquitinating enzyme, cezanne, regulates vascular smooth muscle cell proliferation and migration in arterial remodeling by targeting the β-catenin pathway[29]. Yu and colleagues[30] reported that DUB cylindromatosis causes adventitial fibroblasts to differentiate into myofibroblasts by deubiquitinating nicotinamide adenine dinucleotide phosphate oxidase 4. In our screening of Ang II-responsive USPs in the aorta, we found significantly increased levels of *Usp25*. USP25 was first identified as DUB by Valero et al.[31], and has since been linked to cancer, inflammatory-related diseases, and neurological diseases[14,32,33]. However, studies have not yet linked USP25 to vascular diseases, to our knowledge. This study, for the first time, identifies a USP family member, USP25, as an essential regulator of Ang II-induced vascular remodeling.

FOXO3 is identified as a USP25 target protein in our study. FOXO3 has been reported to regulate a plethora of cellular activities including apoptosis and oxidative stress, which is usually afforded by FOXO3 acting as a PI3K/ATK pathway substrate or interacting with SIRT proteins. Abdullah et al.[34] found that Eugenol can induce autophagy and apoptosis in breast cancer cells by inhibiting the PI3K/AKT/FOXO3a pathway. Jacobs and colleagues showed that SIRT3 can interact with FOXO3 and increase FOXO3-dependent gene expression to affect mitochondrial function[35]. In recent years, the roles of FOXO3 in various vascular diseases have attracted much attention. In smooth muscle cells, FOXO3 suppresses proliferation[36], and in endothelial cells, knocking out FOXO3 causes the emergence of signs of aging[37]. Phosphorylated FOXO3 levels have also been shown in human carotid atherosclerotic plaques[38]. In our study, we found that USP25 protects vascular endothelial cells from Ang II-induced injury by binding FOXO3 and regulating the target protein levels. Interestingly, we find that USP25 interacts with FOXO3 through the USP domain and deubiquitinates FOXO3, which enhances the interaction of FOXO3 with LC3B and leads to FOXO3 degradation. With continued insult and overwhelmed USP25, FOXO3 translocates to the nucleus to regulate the expression of genes involved in EndMT. Therefore, we suggest that the USP25−FOXO3 axis is an important regulatory mechanism in Ang II-induced EndMT. Our study highlights endothelial FOXO3 as an important target in vascular remodeling and adds new understandings to the post-translational modification processes of FOXO3.

$n = 3$; ns = not significant, $^*P < 0.05$). (J) $Usp25^{-/-}$ NIH/3T3 cells were transfected with Flag-USP25, Flag-USP25-C178A, or Flag-USP25-H608A. Flag-vector was used as the control. Lysates were probed for FOXO3 and USP25. (K) $Usp25^{-/-}$ NIH/3T3 cells transfected with Flag-USP25-C178A and His-FOXO3 were cultured in EBSS for various time points. Lysates were probed for His and Flag tags. (L) Densitometric quantification of FOXO3 from Panel (K) (mean ± SEM; $n = 3$; ns = not significant, $^*P < 0.05$). (M, N) $Usp25^{-/-}$ NIH/3T3 cells were transfected with His-FOXO3 and HA-LC3B (M) or His-FOXO3 and HA-P62 (N). Vectors alone were used as the control. His-tag was used for immunoprecipitation and HA-tag for immunoblotting. (O) $Usp25^{-/-}$ NIH/3T3 cells were transfected with His-FOXO3, HA-LC3B, and Flag-USP25. Cells were then treated with 0.2 μmol/L Baf A1 for 6 h. His-tag was used for immunoprecipitation and HA-tag for immunoblotting. Student's *t*-test (unpaired, two-tailed) for (B, C, I, L). One-way ANOVA followed by Tukey's *post hoc* test for (E, F).

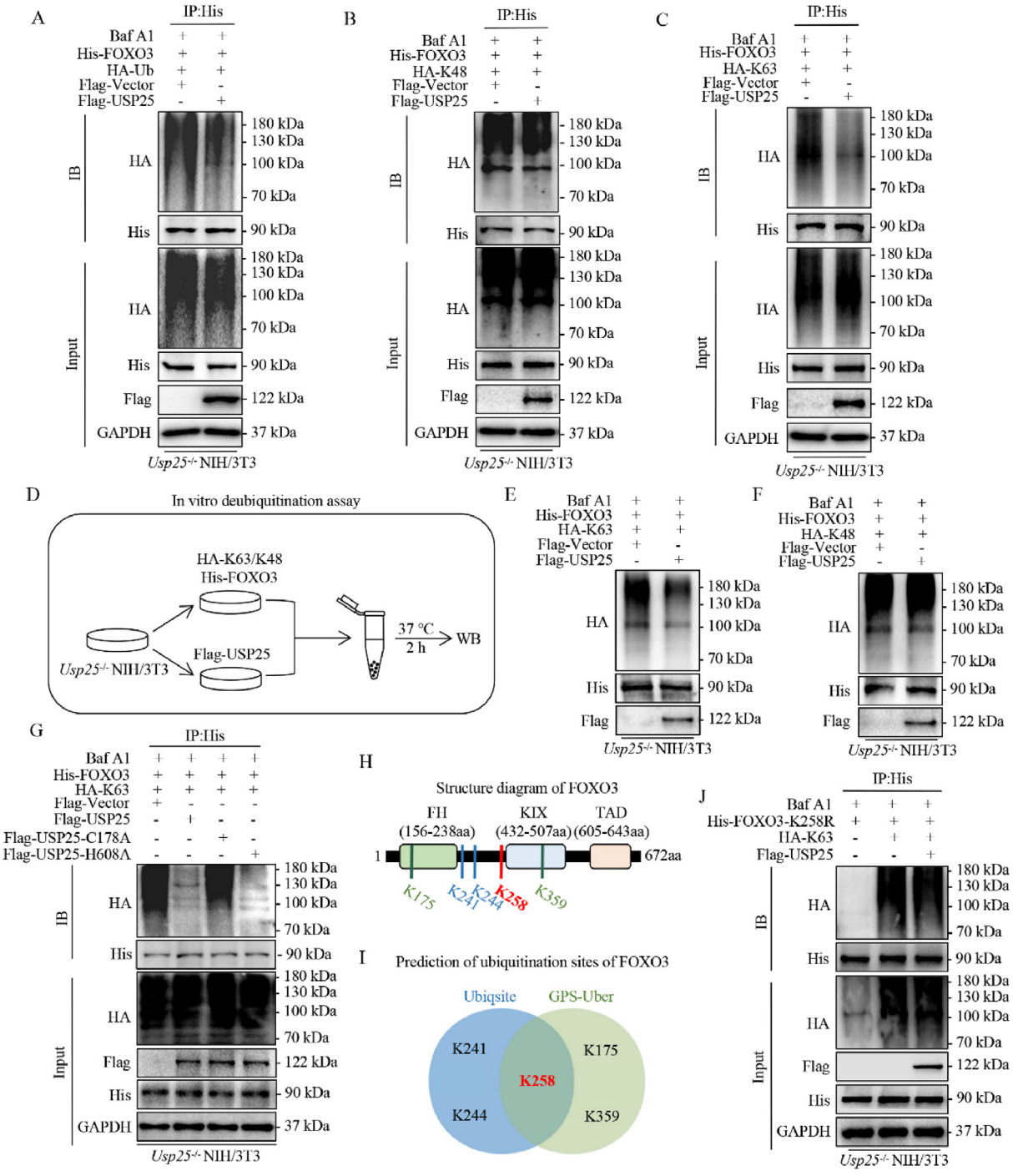

Figure 5 USP25 reverses the K63-linked ubiquitination of lysine 258 on FOXO3. (A–C) *Usp25*$^{-/-}$ NIH/3T3 cells were transfected with Flag-USP25, His-FOXO3, and either HA-Ub (A), HA-K48 (B), or HA-K63 (C). Following transfection, cells were treated with 0.2 μmol/L Baf A1 for 6 h. Lysates were used for co-immunoprecipitation. Ubiquitinated FOXO3 was detected by immunoblotting. (D) Schematic showing the *in vitro* deubiquitinating assay. (E, F) *Usp25*$^{-/-}$ NIH/3T3 cells transfected with various vectors were used for an *in vitro* deubiquitination assay. Cells were exposed to 0.2 μmol/L Baf A1 for 6 h and ubiquitinated FOXO3 was detected. (G) *Usp25*$^{-/-}$ NIH/3T3 cells were transfected with His-FOXO3, HA-K63, and either Flag-USP25, Flag-USP25-C178A, or Flag-USP25-H608A. Cells were then treated with 0.2 μmol/L Baf A1 for 6 h and K63-linked FOXO3 ubiquitination was detected. (H, I) FOXO3 ubiquitination. Figure showing a schematic of FOXO3 structure (H) and predicted ubiquitination sites (I). (J) *Usp25*$^{-/-}$ NIH/3T3 cells were transfected with His-FOXO3-K258R and HA-K63. An additional group included cells co-transfected with Flag-USP25. Following transfections, cells were treated with 0.2 μmol/L Baf A1 for 6 h. Ubiquitinated FOXO3 was detected.

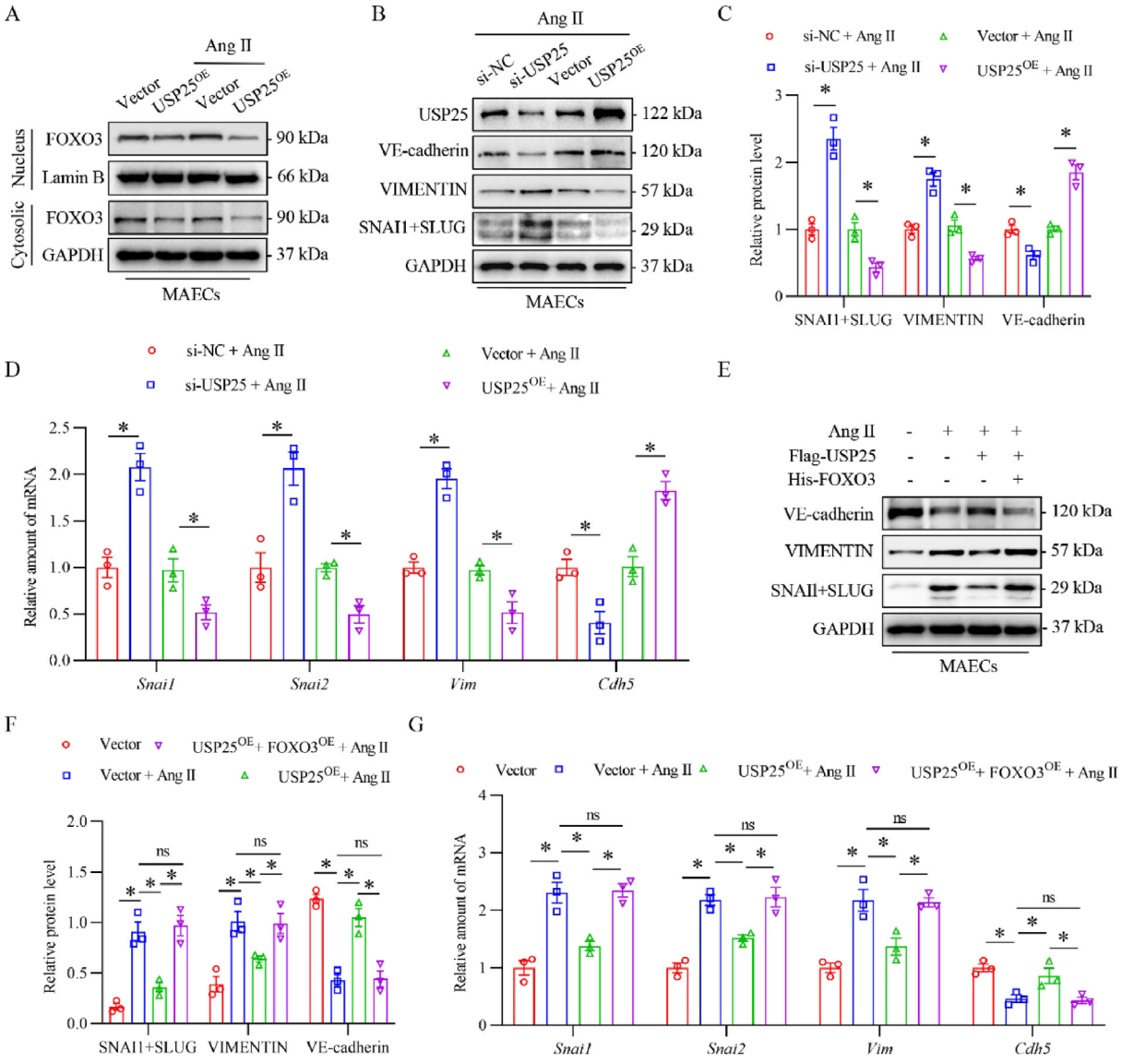

Figure 6 USP25 impacts EndMT by regulating FOXO3 in endothelial cells. (A) MAECs were transfected with Flag-USP25. Cells were then challenged with 1 μmol/L Ang II for 48 h. Lysates were used to measure nuclear and cytosolic FOXO3. Lamin B and GAPDH were used as the loading control. (B) MAECs were transfected with Flag-USP25 to express *Usp25* or siRNA to knockdown *Usp25*. Cells were then exposed to 1 μmol/L Ang II for 48 h. Levels of EndMT markers were measured by immunoblotting. GAPDH was used as the loading control. (C) Densitometric quantification of EndMT markers in MAECs from Panel (B) (mean ± SEM; $n = 3$; $^*P < 0.05$). (D) mRNA levels of genes associated with EndMT. Cells were treated as indicated in Panel (B). Data normalized to *Actb* (mean ± SEM; $n = 3$; $^*P < 0.05$). (E, F) MAECs were transfected with Flag-USP25 and His-FOXO3. Cells were then exposed to 1 μmol/L Ang II for 48 h. Levels of EndMT markers were detected by immunoblotting (E). GAPDH was used as the loading control. Densitometric quantification is shown in panel (F) (mean ± SEM; $n = 3$; ns = not significant, $^*P < 0.05$). (G) mRNA levels of genes associated with EndMT. Cells were treated as indicated in Panel (E). Data normalized to *Actb* (mean ± SEM; $n = 3$; ns = not significant, $^*P < 0.05$). One-way ANOVA followed by Tukey's *post hoc* test for (C, D, F, G).

The linkage type of ubiquitin molecules on a substrate protein determines the outcome of the target protein. Ubiquitin is linked to different lysine residues and methionine residues, resulting in seven types of ubiquitin chains: M1, K6, K11, K27, K29, K33, K48, K63. Studies have shown that USP25 mainly regulates K48 and K63 chains on target proteins[39,40]. For example, USP25 promotes endotoxin tolerance by removing K48-linked ubiquitination of TNF receptor-associated factor-3 in Kupffer cells[41]. LPS-induced increase in USP25 enhances HBO1 stability by removing ubiquitin chains from HBO1 in THP-1 monocytes[42]. Furthermore, these studies did not explore the active site of USP25 in regulating the target protein. In our study, we found that USP25 can exert deubiquitinating activity on FOXO3 *via* the cysteine 178 site to remove K63-linked ubiquitin chain on lysine 258 on FOXO3. This activity facilitates the association of FOXO3 with autophagy-associated LC3B, thereby inducing the degradation of FOXO3 *via* the autophagy pathway. USP25 has been reported to stabilize SERCA2[16], HIF-1α[43], and KEAP1[44] through directly interacts with and deubiquitinating these substrate proteins, respectively. Interestingly, our research found that USP25 can promote autophagy-dependent degradation of FOXO3 by removing its K63-linked ubiquitin chain. This is the first time to

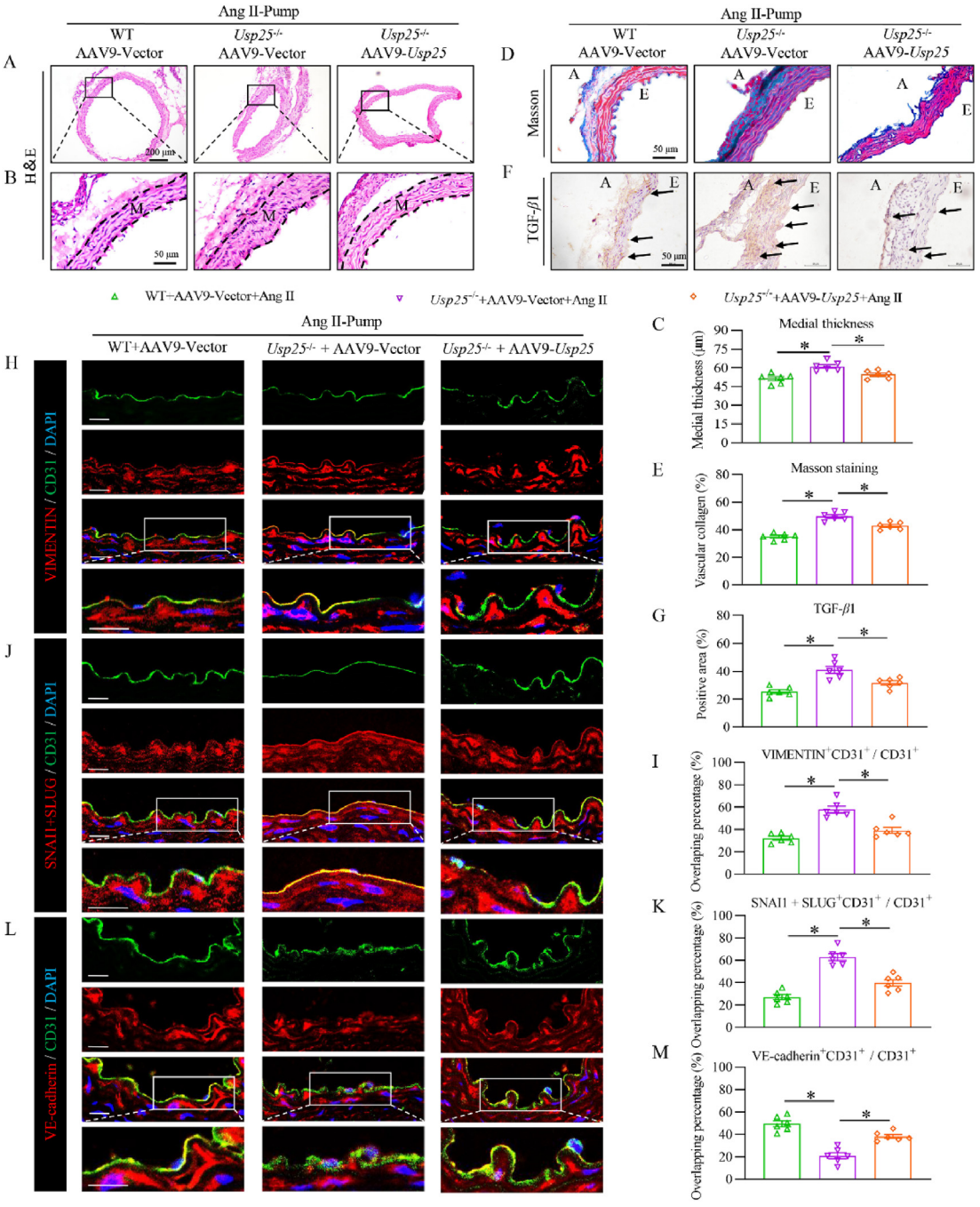

Figure 7 USP25 induction suppresses Ang II-induced vascular remodeling. *Usp25*$^{-/-}$ mice were administered AAV9 expressing *Usp25*. Empty AAV9 was administered in WT and *Usp25*$^{-/-}$ mice as the control. Mice were then infused with Ang II for 4 weeks. (A, B) Representative low-power (A) and high-power (B) images of aortas stained with H&E (Scale bar = 200 μm in panel (A), 50 μm in panel (B); M = media). (C) Quantification of medial thickness in mice determined from H&E-stained sections (mean ± SEM; $n = 6$; $^*P < 0.05$). (D, E) Aortic tissues were stained with Masson's Trichrome. Representative staining images are shown in panel (D) (Scale bar = 50 μm; E = endothelium, A = adventitia). Quantification of collagen from Masson's Trichrome-stained sections is shown in panel (E) (mean ± SEM; $n = 6$; $^*P < 0.05$). (F, G) Representative immunohistochemical staining for TGF-β1 (brown) in aortas are shown in panel (F) (Scale bar = 50 μm; E = endothelium, A = adventitia). Quantification of positive area from immunohistochemical sections of TGF-β1 is shown in panel G (mean ± SEM; $n = 6$; ns = not significant, $^*P < 0.05$). (H, I) Representative double immunofluorescence staining images showing expression of VIMENTIN (red) and CD31 (green) in panel (H). Sections were counterstained with DAPI (blue). Proportion of overlapping area is shown in (I) (Scale bar = 20 μm). (J, K) Representative double immunofluorescence staining images showing expression of SNAI1+SLUG (red) and CD31 (green) in panel (J). Sections were counterstained with DAPI (blue). The proportion of overlapping area is shown in (K) (Scale bar = 20 μm). (L, M) Representative double immunofluorescence staining images showing expression of VE-cadherin (red) and CD31 (green) in panel (L). Sections were counterstained with DAPI (blue). The proportion of overlapping area is shown in (M) (Scale bar = 20 μm). One-way ANOVA followed by Tukey's *post hoc* test for (C, E, G, I, K, M).

report that USP25 can promote the degradation of target protein. Due to the high specificity of the deubiquitination process, the design and development of specific agents through the specific sites of USP25 and FOXO3 may be an interesting direction. These two sites, one of USP25 and one on FOXO3, could potentially be utilized clinically to dampen excessive vascular remodeling features such as fibrosis and EndMT.

There are a few limitations of our study. First, we do not know exactly why and how Ang II administration upregulated USP25 in vascular remodeling. In our study, deficiency in *Usp25* increased the adverse reactions of Ang II exposure. Therefore, it appears that upregulated USP25 may represent a response to counter Ang II signaling and downstream effects. The second limitation relates to our use of global *Usp25* knockout mice. We showed that Ang II-mediated vascular remodeling is increased in global *Usp25* deficient mice. In contrast, restoration of USP25 in global deficient mice reverses the pathological process described above. We also showed that Ang II-induced upregulation of USP25 only occurred in endothelial cells, but not in smooth muscle cells. However, we acknowledge that using endothelial-specific *Usp25* knockout mice may help to provide conclusive evidence. Furthermore, USP25 is a multifunctional deubiquitinating enzyme and may affect non-classical ubiquitination types such as K11, K27, K29, and K33, in addition to classical chain K48 and K63 on FOXO3 protein. This also should be investigated in future studies.

5. Conclusions

In conclusion, we have demonstrated that USP25 induction suppresses Ang II-induced vascular remodeling by modulating the deubiquitination and stability of FOXO3. To our knowledge, this is the first empirical evidence of a potential protective function of USP25 in deleterious vascular remodeling. More importantly, our results suggest that inducing USP25 in patients suffering from hypertension and possibly other vascular diseases may be an effective therapeutic strategy. In this regard, the development of USP25 agonists would be exciting to explore for the treatment of vascular diseases.

Acknowledgments

This study was supported by the National Natural Science Foundation of China (82370244 to Yi Wang, 82361138563 to Yi Wang, and 82271347 to Gaojun Wu), Natural Science Foundation of Zhejiang Province (LY22H070004 to Wu Luo), and Wenzhou City Research Project (ZY2020016 to Gaojun Wu).

Author contributions

Yanghao Chen: Writing − review & editing, Writing − original draft, Visualization, Validation, Software, Project administration, Investigation, Conceptualization. Bozhi Ye: Visualization, Validation, Supervision, Project administration, Formal analysis, Data curation. Diyun Xu: Validation, Software, Resources, Methodology, Conceptualization. Wante Lin: Visualization, Validation, Resources, Methodology. Zimin Fang: Methodology, Investigation, Formal analysis, Data curation. Xuefeng Qu: Validation, Resources, Methodology, Conceptualization. Xue Han: Validation, Methodology, Investigation. Wu Luo: Writing − review & editing, Writing − original draft, Supervision, Project administration, Funding acquisition, Conceptualization. Chen Chen: Visualization, Validation, Formal analysis, Conceptualization. Weijian Huang: Writing − review & editing, Supervision, Methodology, Conceptualization. Hao Zhou: Writing − review & editing, Writing − original draft, Visualization, Validation, Software. Gaojun Wu: Writing − review & editing, Writing − original draft, Supervision, Project administration, Funding acquisition, Conceptualization. Yi Wang: Writing − review & editing, Writing − original draft, Supervision, Project administration, Methodology, Funding acquisition, Conceptualization. Guang Liang: Writing − review & editing, Writing − original draft, Supervision, Resources, Project administration, Investigation, Funding acquisition, Conceptualization.

Conflicts of interest

The authors declare no conflicts of interest.

Appendix A. Supporting information

Supporting information to this article can be found online at https://doi.org/10.1016/j.apsb.2024.12.033.

References

1. Brown I, Diederich L, Good M, DeLalio L, Murphy S, Cortese Krott M, et al. Vascular smooth muscle remodeling in conductive and resistance arteries in hypertension. *Arterioscler Thromb Vasc Biol* 2018;**38**:1969−85.
2. Nur Farah MA, Maarten PK, Jinwei Z. Regulatory control of the Na−Cl co-transporter NCC and its therapeutic potential for hypertension. *Acta Pharm Sin B* 2021;**11**:1117−28.
3. Lu S, Strand K, Mutryn M, Tucker R, Jolly A, Furgeson S, et al. PTEN (phosphatase and tensin homolog) protects against Ang II (angiotensin II)-induced pathological vascular fibrosis and remodeling-brief report. *Arterioscler Thromb Vasc Biol* 2020;**40**:394−403.
4. Bai C, Su M, Zhang YH, Lin YH, Sun YY, Song L, et al. Oviductal glycoprotein 1 promotes hypertension by inducing vascular remodeling through an interaction with MYH9. *Circulation* 2022;**146**:1367−82.
5. Gan L, Liu D, Liu J, Chen E, Chen C, Liu L, et al. CD38 deficiency alleviates Ang II-induced vascular remodeling by inhibiting small extracellular vesicle-mediated vascular smooth muscle cell senescence in mice. *Signal Transduct Target Ther* 2021;**6**:223.
6. Gao P, Xu TT, Lu J, Li L, Xu J, Hao DL, et al. Overexpression of SIRT1 in vascular smooth muscle cells attenuates angiotensin II-induced vascular remodeling and hypertension in mice. *J Mol Med Berl* 2014;**92**:347−57.
7. Good RB, Gilbane AJ, Trinder SL, Denton CP, Coghlan G, Abraham DJ, et al. Endothelial to mesenchymal transition contributes to endothelial dysfunction in pulmonary arterial hypertension. *Am J Pathol* 2015;**185**:1850−8.
8. Xing YJ, Hou YF, Fan TF, Ran G, Feng XH, Li BL, et al. Endothelial phosphodiesterase 4B inactivation ameliorates endothelial-to-mesenchymal transition and pulmonary hypertension. *Acta Pharm Sin B* 2024;**14**:1726−41.
9. You SB, Qian JC, Wu GJ, Qian YY, Wang ZX, Chen TW, et al. Schizandrin B attenuates angiotensin II induced endothelial to mesenchymal transition in vascular endothelium by suppressing NF-κB activation. *Phytomedicine* 2019;**62**:152955.
10. Qian JF, Luo WL, Dai CY, Wang J, Guan XF, Zou CP, et al. Myeloid differentiation protein 2 mediates angiotensin II-induced inflammation and mesenchymal transition in vascular endothelium. *Biochim Biophys Acta, Mol Basis Dis* 2021;**1867**:166043.
11. Komander D, Rape M. The ubiquitin code. *Annu Rev Biochem* 2012;**81**:203−29.

12. Nijman SM, Luna Vargas MP, Velds A, Brummelkamp TR, Dirac AM, Sixma TK, et al. A genomic and functional inventory of deubiquitinating enzymes. *Cell* 2005;**123**:773−86.
13. Chen RR, Pang XB, Li L, Zeng ZR, Chen MH, Zhang SH. Ubiquitin-specific proteases in inflammatory bowel disease-related signalling pathway regulation. *Cell Death Dis* 2022;**13**:139.
14. Nelson J, Thin M, Evan T, Howell S, Wu M, Almeida B, et al. USP25 promotes pathological HIF-1-driven metabolic reprogramming and is a potential therapeutic target in pancreatic cancer. *Nat Commun* 2022;**13**:2070.
15. Zhu HR, Gao YM, Liu LY, Tao MY, Lin X, Cheng YJ, et al. A novel TNKS/USP25 inhibitor blocks the Wnt pathway to overcome multidrug resistance in TNKS-overexpressing colorectal cancer. *Acta Pharm Sin B* 2024;**14**:207−22.
16. Ye BZ, Zhou H, Chen YH, Luo W, Lin WT, Zhao Y, et al. USP25 ameliorates pathological cardiac hypertrophy by stabilizing SERCA2a in cardiomyocytes. *Circ Res* 2023;**132**:465−80.
17. Wang JM, Chen AF, Zhang KZ. Isolation and primary culture of mouse aortic endothelial cells. *J Vis Exp* 2016;**118**:52965.
18. Chi JF, Meng LP, Pan SL, Lin H, Zhai XY, Liu LB, et al. Primary culture of rat aortic vascular smooth muscle cells: a new method. *Med Sci Monit* 2017;**23**:4014−20.
19. Huang ZQ, Shen SR, Wang MY, Li WX, Wu GJ, Huang WJ, et al. Mouse endothelial OTUD1 promotes angiotensin II-induced vascular remodeling by deubiquitinating SMAD3. *EMBO Rep* 2023;**24**:e56135.
20. Huang GJ, Cong ZL, Wang XY, Yuan YG, Xu RJ, Lu ZY, et al. Targeting HSP90 attenuates angiotensin II-induced adventitial remodelling *via* suppression of mitochondrial fission. *Cardiovasc Res* 2019;**116**:1071−84.
21. Lin K, Luo W, Yan JQ, Shen SY, Shen QR, Wang J, et al. TLR2 regulates angiotensin II-induced vascular remodeling and EndMT through NF-κB signaling. *Aging (Albany NY)* 2020;**13**:2553−74.
22. Xu L, Fu MG, Chen DR, Han WQ, Ostrowski MC, Grossfeld P, et al. Endothelial-specific deletion of Ets-1 attenuates Angiotensin II-induced cardiac fibrosis *via* suppression of endothelial-to-mesenchymal transition. *BMB Rep* 2019;**52**:595−600.
23. Hamid EK, Elnaz T, Shahram RD. Abdominal pain as extrapulmonary presentation of pneumonia in an adult: a case report. *Acta Med Iran* 2017;**55**:131−3.
24. Diebold I, Petry A, Burger M, Hess J, Görlach A. NOX4 mediates activation of FOXO3a and matrix metalloproteinase-2 expression by urotensin-II. *Mol Biol Cell* 2011;**22**:4424−34.
25. Issa A, Sun J, Petitgas C, Mesquita A, Dulac A, Robin M, et al. The lysosomal membrane protein LAMP2A promotes autophagic flux and prevents SNCA-induced Parkinson disease-like symptoms in the *Drosophila* brain. *Autophagy* 2018;**14**:1898−910.
26. Liu B, Sureda Gomez M, Zhen Y, Amador V, Reverter D. A quaternary tetramer assembly inhibits the deubiquitinating activity of USP25. *Nat Commun* 2018;**9**:4973.
27. Coda D, Patel H, Gori I, Gaarenstroom T, Song O, Howell M, et al. A network of transcription factors governs the dynamics of NODAL/Activin transcriptional responses. *J Cell Sci* 2022;**135**:jcs259972.
28. Weber T. Anti-AAV antibodies in AAV gene therapy: current challenges and possible solutions. *Front Immunol* 2021;**12**:658399.
29. An WW, Luong LA, Bowden NP, Yang M, Wu W, Zhou XM, et al. Cezanne is a critical regulator of pathological arterial remodelling by targeting β-catenin signalling. *Cardiovasc Res* 2022;**118**:638−53.
30. Yu B, Liu ZY, Fu Y, Wang YB, Zhang L, Cai ZY, et al. CYLD deubiquitinates nicotinamide adenine dinucleotide phosphate oxidase 4 contributing to adventitial remodeling. *Arterioscler Thromb Vasc Biol* 2017;**37**:1698−709.
31. Valero R, Marfany G, González Angulo O, González González G, Puelles L, Gonzàlez Duarte R. USP25, a novel gene encoding a deubiquitinating enzyme, is located in the gene-poor region 21q11.2. *Genomics* 1999;**62**:395−405.
32. Liu ZR, Qi MM, Tian S, Yang Q, Liu J, Wang SW, et al. Ubiquitin-specific protease 25 aggravates acute pancreatitis and acute pancreatitis-related multiple organ injury by destroying tight junctions through activation of the STAT3 pathway. *Front Cell Dev Biol* 2021;**9**:806850.
33. Zheng QY, Li GL, Wang SH, Zhou Y, Liu K, Gao Y, et al. Trisomy 21-induced dysregulation of microglial homeostasis in Alzheimer's brains is mediated by USP25. *Sci Adv* 2021;**7**:eabe1340.
34. Abdullah M, Al Shabanah O, Hassan Z, Hafez M. Eugenol-induced autophagy and apoptosis in breast cancer cells *via* PI3K/AKT/FOXO3a pathway inhibition. *Int J Mol Sci* 2021;**22**:9243.
35. Jacobs K, Pennington J, Bisht K, Aykin Burns N, Kim H, Mishra M, et al. SIRT3 interacts with the daf-16 homolog FOXO3a in the mitochondria, as well as increases FOXO3a dependent gene expression. *Int J Biol Sci* 2008;**4**:291−9.
36. Lee HY, Chung JW, Youn SW, Kim JY, Park KW, Koo BK, et al. Forkhead transcription factor FOXO3a is a negative regulator of angiogenic immediate early gene CYR61, leading to inhibition of vascular smooth muscle cell proliferation and neointimal hyperplasia. *Circ Res* 2007;**100**:372−80.
37. Zhang WQ, Zhang S, Yan PZ, Ren J, Song MS, Li JY, et al. A single-cell transcriptomic landscape of primate arterial aging. *Nat Commun* 2020;**11**:2202.
38. Wang C, Wen JY, Zhou Y, Li L, Cui XB, Wang JY, et al. Apelin induces vascular smooth muscle cells migration *via* a PI3K/Akt/FoxO3a/MMP-2 pathway. *Int J Biochem Cell Biol* 2015;**69**:173−82.
39. Zhong HJ, Wang D, Fang LR, Zhang H, Luo R, Shang M, et al. Ubiquitin-specific proteases 25 negatively regulates virus-induced type I interferon signaling. *PLoS One* 2013;**8**:e80976.
40. Shi L, Wen Y, Zhang NX. ^{1}H, ^{13}C and ^{15}N backbone and side-chain resonance assignments of the N-terminal ubiquitin-binding domains of USP25. *Biomol NMR Assign* 2014;**8**:255−8.
41. Wen J, Bai H, Chen N, Zhang WF, Zhu XW, Li PZ, et al. USP25 promotes endotoxin tolerance *via* suppressing K48-linked ubiquitination and degradation of TRAF3 in Kupffer cells. *Mol Immunol* 2019;**106**:53−62.
42. Long C, Lai YD, Li J, Huang JS, Zou CB. LPS promotes HBO1 stability *via* USP25 to modulate inflammatory gene transcription in THP-1 cells. *Biochim Biophys Acta Gene Regul Mech* 2018;**1861**:773−82.
43. Jessica KN, May Zaw T, Theodore E, Steven H, Mary W, Bruna A, et al. USP25 promotes pathological HIF-1-driven metabolic reprogramming and is a potential therapeutic target in pancreatic cancer. *Nat Commun* 2022;**13**:2070.
44. Cai CZ, Ma HL, Peng J, Shen X, Zhen XH, Yu CH, et al. USP25 regulates KEAP1−NRF2 anti-oxidation axis and its inactivation protects acetaminophen-induced liver injury in male mice. *Nat Commun* 2023;**14**:3648.